Check for updates

Amyloid fibril-UiO-66-NH$_2$ aerogels for environmental remediation†

Mohammad Peydayesh, [ID] [a] Xiulin Chen,[a] Julia Vogt,[a] Felix Donat, [ID] [b]
Christoph R. Müller [ID] [b] and Raffaele Mezzenga [ID] *[ac]

A sustainable hybrid aerogel based on β-lactoglobulin amyloid fibril/UiO-66-NH$_2$ is developed for environmental remediation. The hybrid aerogel's CO$_2$ capture and water purification performances were investigated. The hybrid aerogel can achieve CO$_2$ capture and possesses excellent adsorption capacities for several heavy metals, dyes, and organic solvents.

Toxic pollutants, such as heavy metals and organic compounds, impart deleterious effects on human health and thus trigger global concerns.[1,2] In addition, the planetary boundary of climate change has already been exceeded, and is causing irreversible damage to the Earth.[3] Therefore, several water purification and CO$_2$ capture approaches have been introduced.[4,5] Although these technologies are both reliable and efficient, they are not sustainable due to high energy demands and costs.[6] Therefore, developing sustainable and environmentally-friendly technologies is crucial. Metal–organic frameworks (MOFs) are highly porous nanostructures comprising metal ions/clusters and organic linkers[7] with exceptional characteristics, such as high porosity and surface area, diversity, and flexibility.[8] These properties enable MOFs to possess superior potential in adsorption,[9] gas capture,[10] and separation,[11] as well as environmental remediation.[12] Zirconium-based MOFs, UiO-66, and UiO-66-NH$_2$ have high hydrothermal stability,[13] which is beneficial for water applications. Furthermore, amino groups in UiO-66-NH$_2$ allow for CO$_2$ adsorption properties.[14] However, certain limitations exist for direct application of powdered MOFs, such as poor processability due to fragile and crystalline structures,[12] as well

as aggregation issues.[7] We hereby design hybrid MOF-amyloid fibril materials capable to meet the above challenges.

Amyloid fibrils can be prepared by self-assembly of various proteins under proper denaturation and hydrolysis conditions.[15] Different advanced materials based on amyloid fibrils have been developed, such as aerogels, hydrogels, and membranes.[2,16,17] Indeed, it has been shown that amyloid fibrils can remove microplastics,[18] heavy metals,[1] dyes, and organic matter[2] from water. In this study, β-lactoglobulin (β-Lg) was used to produce amyloid fibrils, since it is not only the most abundant protein in whey (a by-product of cheese manufacturing), but it is also a globular protein that can easily self-assemble into amyloid fibrils.[19] The hybrid UiO-66-NH$_2$/β-Lg amyloid fibrils aerogel is subsequently studied for two critical environmental applications: CO$_2$ capture and water purification.

The hybrid aerogel was prepared by a green and straightforward protocol, schematically described in Fig. 1a, with the details elaborated in the experimental section. The morphology and structure of UiO-66-NH$_2$ were assessed by TEM analysis (Fig. 1b), showing the octahedral shape of UiO-66-NH$_2$ with a particle size in the range of 80–100 nm. The element mapping images of UiO-66-NH$_2$ in Fig. 1c indicate that the elements Zr, C, N, and O were distributed uniformly in the composite. As shown in Fig. S1a (ESI†), the N$_2$ sorption isotherm of UiO-66-NH$_2$ was type IV, indicating a microporous structure and more than 60% of the pore volume is linked with the pores smaller than 2 nm. The N$_2$ sorption results are presented in Table S1 (ESI†). The N$_2$ sorption isotherm and the surface area, pore radius, and pore volume of the hybrid aerogels are shown in Fig. S1b and Table S1 (ESI†). As shown in Fig. S2 (ESI†), the isoelectric point for UiO-66-NH$_2$ was reached when the pH value was approximately 3.4. UiO-66-NH$_2$ had positive charges at the condition of pH 2 amyloid fibrils solution, which is beneficial for the adsorption of negatively-charged molecules and compounds.

In Fig. 2a, the hybrid aerogel's homogenous and highly porous structure can be observed by SEM. Fig. 2b and Fig. S3 (ESI†) demonstrate the distribution of the regular-shaped

[a] *Department of Health Sciences and Technology, ETH Zurich, Schmelzbergstrasse 9, 8092 Zurich, Switzerland. E-mail: raffaele.mezzenga@hest.ethz.ch; Tel: +41 44 632 9140*

[b] *Department of Mechanical and Process Engineering, ETH Zurich, Leonhardstrasse 21, 8092 Zurich, Switzerland*

[c] *Department of Materials, ETH Zurich, Wolfgang-Pauli-Strasse 10, 8093 Zurich, Switzerland*
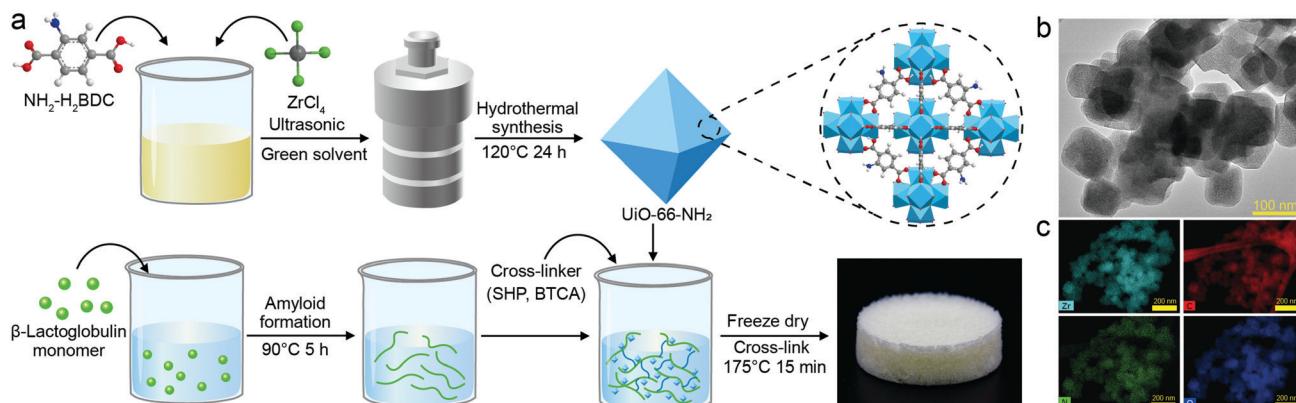
Fig. 1 Fabrication process of hybrid UiO-66-NH$_2$ and amyloid fibrils aerogel. (a) Schematic of UiO-66-NH$_2$ synthesis, and the preparation process of the hybrid aerogel. Morphological features of UiO-66-NH$_2$. (b) TEM image of UiO-66-NH$_2$. (c) Elemental maps of UiO-66-NH$_2$.
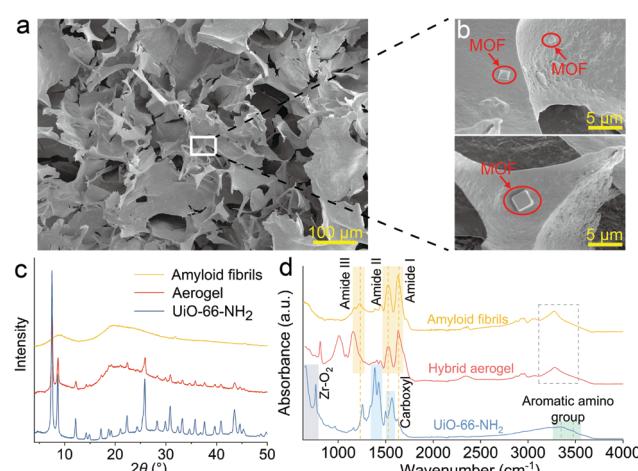

Fig. 2 Characterization of the hybrid aerogel. (a and b) SEM images of the inner structure of the hybrid aerogel. (c) The XRD patterns and (d) FTIR spectra of amyloid fibrils, hybrid aerogels, and UiO-66-NH$_2$.

UiO-66-NH$_2$ particles on the amyloid network surface. The hybrid aerogels were ultralight and robust, the density was approximately 40 mg cm^{-3}, and the Young's modulus was approximately $E = 2.0 \times 10^{-2}$ MPa (Table S2, ESI†). The compressive strain and stress curve of the hybrid aerogel is shown in Fig. S4 (ESI†). XRD patterns presented in Fig. 2c reveal the purity and crystallinity of the materials. The pattern of amyloid fibrils had no diffraction peaks and exhibited a broad amorphous peak due to β-Lg.[20] The pattern of UiO-66-NH$_2$ was in accordance with previous literature,[21,22] indicating that pure and crystalline UiO-66-NH$_2$ was successfully synthesized. The pattern contains the characteristic main peaks of UiO-66 at $2\theta = 7.34°$ and $8.48°$.[23] Moreover, the presence of the –NH$_2$ group in UiO-66 did not affect the XRD pattern due to the MOF structure.[24] In the pattern of the hybrid aerogel, the same characteristic peaks of UiO-66-NH$_2$ can be seen, suggesting that the hybridization with amyloid fibrils did not influence the crystal structure of UiO-66-NH$_2$. Given the amorphous nature of the MOF/amyloid interface, high-resolution

techniques such as gel-state NMR spectroscopy can be considered for future studies to provide additional insights regarding local structures and interactions.[25–27] The thermal stability of the aerogel was evaluated by thermogravimetric analysis (TGA) and shown in Fig. S5 (ESI†). No significant weight change was observed in N$_2$ or air up to 250 °C, indicating a good thermal stability of the hybrid aerogel. The interaction between amyloid fibrils and UiO-66-NH$_2$ was also investigated using FTIR spectroscopy (Fig. 2d). For UiO-66-NH$_2$, the bands at 3475 and 3363 cm^{-1} can be assigned to N–H symmetric and asymmetric vibrations, respectively.[28] A wide and medium absorbance feature at approximately 3300 cm^{-1} proves the existence of H-bonded hydroxyls. The absorption band at 1570 cm^{-1} indicates the presence of the reaction of –COOH with Zr.[21] The doublet at 1421 and 1387 cm^{-1} are attributed to the stretching modes of the carboxylic groups in the organic linker.[29] The bands at 1337 and 1258 cm^{-1} are due to C$_{aromatic}$–N vibration.[30] The observed peaks between 600–800 cm^{-1} represent Zr–O$_2$ as longitudinal and transverse modes.[31] The FTIR spectrum of amyloid fibrils exhibits the amide I region at 1630 cm^{-1}, reflecting C=O stretching vibration and the amide II region at 1525 cm^{-1}, due to N–H bending vibration and C–N stretching vibration, and the amide III region at 1230 cm^{-1} in the protein.[32] The broad peak at approximately 3270 cm^{-1} can be ascribed to the –OH vibration.[33] The slight shifts of peaks in the hybrid aerogel pattern can be attributed to the formation of hydrogen bonds between amyloid fibrils and UiO-66-NH$_2$ at the interface.[24] Furthermore, two new peaks in the region between 900–1200 cm^{-1} appear which are tentatively attributed to the shift of carboxyl stretch of UiO-66-NH$_2$, caused by the interaction of amyloid fibrils and UiO-66-NH$_2$.[34]

Fig. 3 presents the CO$_2$ capture performance of hybrid aerogels for different loadings of UiO-66-NH$_2$ near ambient temperature. The CO$_2$ uptake of the pure UiO-66-NH$_2$ and the hybrid aerogels containing 30%, 40%, and 50% UiO-66-NH$_2$ (weight percentage) were 1.14, 0.11, 0.16, and 0.25 mmol g^{-1}, respectively. The performance of pure UiO-66-NH$_2$ was comparable with published data of approximately 1.6 mmol g^{-1}.[35] Measurements of pure amyloid aerogel revealed that amyloid
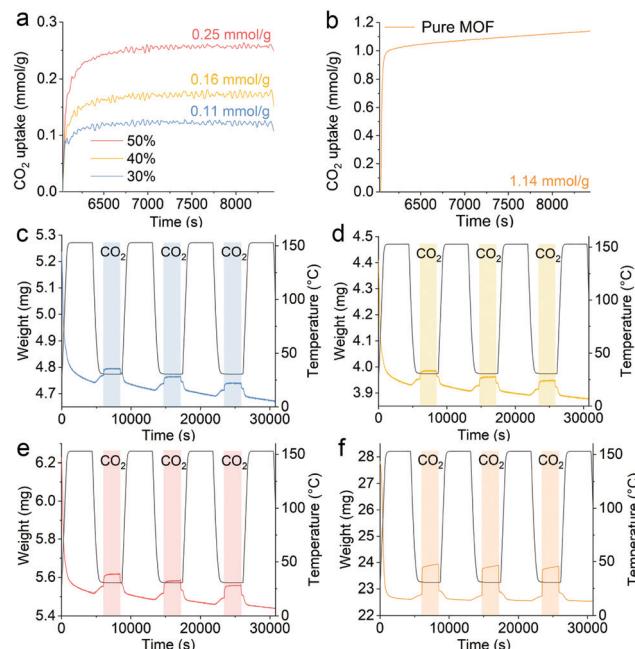
Fig. 3 CO_2 capture performance of (a) hybrid aerogels with different MOF loadings and (b) pure MOF, (c–f) weight changes for three consecutive cycles of CO_2 sorption–desorption of hybrid aerogels with 30%, 40%, 50% MOF and pure MOF, respectively.

Fig. 4 Water purification performance. (a) Reduced Au^{3+} into Au nano-particle and metallic gold on top of the aerogel. (b and c) Dye removal performance. (d) Rapid removal of organic solvents from water. (e–g) Changes of adsorption performance after three regeneration cycles.

fibrils make no significant contribution to CO_2 capture (Fig. S6, ESI†), in contrast with previous findings on designed amyloids.[36,37] Therefore, the hybrid aerogels possessed a larger capacity for CO_2 uptake with higher content of UiO-66-NH$_2$. In the hybrid aerogel, while amyloid fibrils act as a robust platform for the materials, UiO-66-NH$_2$ endowed the materials with binding sites for CO_2 capture. The micropores in UiO-66-NH$_2$ favored the transport of CO_2 to binding sites and the retention of CO_2, which is related to physical adsorption. In addition, the interactions of amino groups in UiO-66-NH$_2$ with CO_2 molecules were responsible for CO_2 capture performance.[14] The results demonstrated that the adsorption capacity of the materials was maintained after three consecutive cycles of CO_2 sorption–desorption, confirming the high durability and reversibility of the hybrid aerogels.

Fig. S7 and S8 (ESI†) show the removal performances of the hybrid aerogels for different heavy metals. The mechanism for heavy metal adsorption is mainly attributed to the chemical chelation between amino acids on the amyloid surface and the heavy metal ions.[38] The results revealed that the hybrid aerogels had a much higher capacity for Au^{3+} (547 mg g^{-1}) and Pt^{4+} (186 mg g^{-1}) than the pure amyloid fibrils aerogel. While the hybrid aerogels demonstrated excellent capacity for Cr^{6+} (308 mg g^{-1}) and Fe^{3+} (226 mg g^{-1}), amyloid fibril aerogel showed no capacity for these metals. Additionally, the hybrid aerogels exhibited high removal efficiency for Au^{3+}, Fe^{3+}, and Pt^{4+}. The improved performance of the hybrid aerogel can be ascribed to UiO-66-NH$_2$. The adsorption mechanism of UiO-66-NH$_2$ is expected to be the ion exchange and electrostatic effect of –NH$_2$ and –COOH groups, combined with the material's
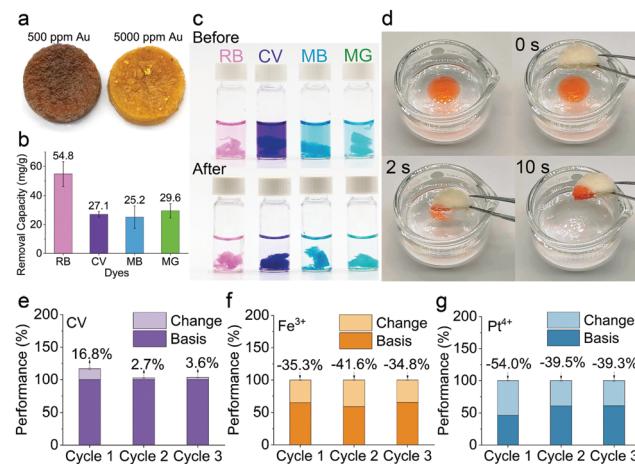
nano-porous structure.[39,40] To investigate the competitive adsorption, the hybrid aerogel was immersed in a mixture solution containing 10 heavy metals, the results of which are presented in Fig. S9 (ESI†). The data demonstrate that the aerogel had high adsorption efficiency for Au^{3+}, Fe^{3+}, and Ag^+. The efficiency for Pt^{4+} was much lower compared with the separately conducted adsorption experiment, which might be because Ag^+ adsorbed faster than Pt^{4+}, and they share the same binding sites. After the adsorption of Ag^+, there were probably fewer binding sites available for Pt^{4+}. Compared with other type of adsorbents (see Table S3, ESI†), the hybrid aerogels in this work exhibited excellent adsorption capacity for Au^{3+}, which could be attributed to the synergies of UiO-66-NH$_2$ and amyloid fibrils. Fig. S10 (ESI†) shows the fitted binding isotherm of Au^{3+}. The hybrid aerogel reduced Au^{3+} into Au nanoparticles and pellets when the concentration of Au^{3+} in solution was 500 ppm and 5000 ppm, respectively (Fig. 4a). The XRD patterns (Fig. S11, ESI†) revealed the characteristic peaks of Au(0),[41] indicating the redox reaction between the hybrid aerogels and Au^{3+}.

The capability of hybrid aerogels for removing organic dyes was also investigated. The results shown in Fig. 4b and c indicate that the removal capacity for Rhodamine B, Crystal violet, Methylene blue, and Malachite green were 54.8, 27.1, 25.2, and 29.6 mg g^{-1}, respectively. The adsorption can be explained mainly by the hydrophobic interactions between the benzene ring of dyes and the hydrophobic domains of the amyloid fibrils.[38] Moreover, Fig. 4d shows the rapid adsorption of n-hexane stained with Oil Red O within 10 s by the hybrid aerogel (ESI† Movie available). The reason for the excellent oil adsorption performance might be that the highly porous structure of the hybrid aerogel provides abundant capillary tunnels that drive the oil to pass through by capillary force rapidly,[42] and the oil remained trapped within interconnected micropores.[43]

To evaluate the reusability of the hybrid aerogels, three subsequent adsorption-regeneration experiments were conducted and the results are presented in Fig. 4e–g. The basis adsorption performances, which means 100%, were obtained from fresh aerogels. The changes in adsorption performance are illustrated by light color in each panel. For Crystal violet, the performance for cycle 1, 2, and 3 increased by 16.8%, 2.7%, and 3.6%, respectively. The performance improvement could be explained by introducing new hydrophobic binding sites by methanol treatment.[2] The washing could also increase the surface area and roughness of the aerogel by removing other impurities.[44] For Fe^{3+} and Pt^{4+}, the performances decreased after washing, which might be because the regeneration cannot remove all of the pollutants, leading to fewer binding sites available for the next cycle.

Conflicts of interest

There are no conflicts to declare.

Notes and references

1 M. Peydayesh, S. Bolisetty, T. Mohammadi and R. Mezzenga, *Langmuir*, 2019, **35**(11), 4161–4170.
2 M. Peydayesh, M. K. Suter, S. Bolisetty, S. Boulos, S. Handschin, L. Nyström and R. Mezzenga, *Adv. Mater.*, 2020, **32**(12), 1907932.
3 J. Rockström, W. Steffen, K. Noone, Å. Persson, F. S. Chapin, E. F. Lambin, T. M. Lenton, M. Scheffer, C. Folke and H. J. Schellnhuber, *Nature*, 2009, **461**(7263), 472–475.
4 A. A. Olajire, *Energy*, 2010, **35**(6), 2610–2628.
5 R. Ghahremani, B. Baheri, M. Peydayesh, S. Asarehpour and T. Mohammadi, *Res. Chem. Intermed.*, 2015, **41**(12), 9845–9862.
6 S. Bolisetty, M. Peydayesh and R. Mezzenga, *Chem. Soc. Rev.*, 2019, **48**(2), 463–487.
7 S. Yu, H. Pang, S. Huang, H. Tang, S. Wang, M. Qiu, Z. Chen, H. Yang, G. Song and D. Fu, *Sci. Total Environ.*, 2021, **800**, 149662.
8 B.-M. Jun, Y. A. Al-Hamadani, A. Son, C. M. Park, M. Jang, A. Jang, N. C. Kim and Y. Yoon, *Sep. Purif. Technol.*, 2020, **247**, 116947.
9 L. Rani, J. Kaushal, A. L. Srivastav and P. Mahajan, *Environ. Sci. Pollut. Res.*, 2020, 1–26.
10 M. Ding, R. W. Flaig, H.-L. Jiang and O. M. Yaghi, *Chem. Soc. Rev.*, 2019, **48**(10), 2783–2828.
11 M. F. Ghazvini, M. Vahedi, S. N. Nobar and F. Sabouri, *J. Environ. Chem. Eng.*, 2020, **9**(1), 104790.
12 R. M. Rego, G. Kuriya, M. D. Kurkuri and M. Kigga, *J. Hazard. Mater.*, 2021, **403**, 123605.
13 Q. Chen, Q. He, M. Lv, Y. Xu, H. Yang, X. Liu and F. Wei, *Appl. Surf. Sci.*, 2015, **327**, 77–85.
14 Y. Cao, H. Zhang, F. Song, T. Huang, J. Ji, Q. Zhong, W. Chu and Q. Xu, *Materials*, 2018, **11**(4), 589.
15 Y. Cao and R. Mezzenga, *Adv. Colloid Interface Sci.*, 2019, **269**, 334–356.
16 M. Usuelli, T. Germerdonk, Y. Cao, M. Peydayesh, M. Bagnani, S. Handschin, G. Nyström and R. Mezzenga, *Nanoscale*, 2021, **13**(29), 12534–12545.
17 T. Jin, M. Peydayesh, H. Joerss, J. Zhou, S. Bolisetty and R. Mezzenga, *Environ. Sci. Water Res. Technol.*, 2021, **7**(10), 1873–1884.
18 M. Peydayesh, T. Suta, M. Usuelli, S. Handschin, G. Canelli, M. Bagnani and R. Mezzenga, *Environ. Sci. Technol.*, 2021, **55**(13), 8848–8858.
19 G. Kontopidis, C. Holt and L. Sawyer, *J. Dairy Sci.*, 2004, **87**(4), 785–796.
20 Z. Chavoshpour-Natanzi and M. Sahihi, *Food Hydrocolloids*, 2019, **96**, 493–502.
21 C. L. Luu, T. T. Van Nguyen, T. Nguyen and T. C. Hoang, *Adv. Nat. Sci.: Nanosci. Nanotechnol.*, 2015, **6**(2), 025004.
22 Y. Wang, H. Chen, X. Hu and H. Yu, *Analyst*, 2016, **141**(15), 4647–4653.
23 J. H. Cavka, S. Jakobsen, U. Olsbye, N. Guillou, C. Lamberti, S. Bordiga and K. P. Lillerud, *J. Am. Chem. Soc.*, 2008, **130**(42), 13850–13851.
24 O. G. Nik, X. Y. Chen and S. Kaliaguine, *J. Membr. Sci.*, 2012, **413**, 48–61.
25 Nonappa and E. Kolehmainen, *Soft Matter*, 2016, **12**(28), 6015–6026.
26 G. M. Reddy, G. M. Peters, B. P. Tatman, T. S. Rajan, S. M. Kock, J. Zhang, B. G. Frenguelli, J. T. Davis, A. Marsh and S. P. Brown, *Mater. Adv.*, 2020, **1**(7), 2236–2247.
27 A. Wickramasinghe, Y. Xiao, N. Kobayashi, S. Wang, K. P. Scherpelz, T. Yamazaki, S. C. Meredith and Y. Ishii, *J. Am. Chem. Soc.*, 2021, **143**(30), 11462–11472.
28 N. Zhang, R. Jin, G. Mao, J. Tan, L. Chen, C. Li and J. Wang, *Inorg. Chim. Acta*, 2021, 120674.
29 X.-Y. Xu, C. Chu, H. Fu, X.-D. Du, P. Wang, W. Zheng and C.-C. Wang, *Chem. Eng. J.*, 2018, **350**, 436–444.
30 K. Chakarova, I. Strauss, M. Mihaylov, N. Drenchev and K. Hadjiivanov, *Microporous Mesoporous Mater.*, 2019, **281**, 110–122.
31 J. Yang, Y. Dai, X. Zhu, Z. Wang, Y. Li, Q. Zhuang, J. Shi and J. Gu, *J. Mater. Chem. A*, 2015, **3**(14), 7445–7452.
32 J. Ioannou, A. Donald and R. Tromp, *Food Hydrocolloids*, 2015, **46**, 216–225.
33 M. Peydayesh, T. Greber, I. Haechler, A. Armanious, X. Jia, M. Usuelli, M. Bagnani and R. Mezzenga, *Adv. Sustainable Syst.*, 2021, 2100309.
34 R. Kardani, M. Asghari, N. F. Hamedani and M. Afsari, *J. Ind. Eng. Chem.*, 2020, **83**, 100–110.
35 Y. Jiang, C. Liu, J. Caro and A. Huang, *Microporous Mesoporous Mater.*, 2019, **274**, 203–211.
36 D. Li, H. Furukawa, H. Deng, C. Liu, O. M. Yaghi and D. S. Eisenberg, *Proc. Natl. Acad. Sci. U. S. A.*, 2014, **111**(1), 191–196.
37 D. Li, E. M. Jones, M. R. Sawaya, H. Furukawa, F. Luo, M. Ivanova, S. A. Sievers, W. Wang, O. M. Yaghi and C. Liu, *J. Am. Chem. Soc.*, 2014, **136**(52), 18044–18051.
38 M. Peydayesh and R. Mezzenga, *Nat. Commun.*, 2021, **12**(1), 1–17.
39 F. Zhao, C. Su, W. Yang, Y. Han, X. Luo, C. Li, W. Tang, T. Yue and Z. Li, *Appl. Surf. Sci.*, 2020, **527**, 146862.
40 Y. Zhang, X. Xu, C. Yue, L. Song, Y. Lv, F. Liu and A. Li, *Chem. Eng. J.*, 2021, **404**, 126546.
41 J. Guo, X. Fan, J. Wang, S. Yu, M. Laipan, X. Ren, C. Zhang, L. Zhang and Y. Li, *Chem. Eng. J.*, 2021, 130588.
42 Q. Zhu, Y. Chu, Z. Wang, N. Chen, L. Lin, F. Liu and Q. Pan, *J. Mater. Chem. A*, 2013, **1**(17), 5386–5393.
43 N. Chen and Q. Pan, *ACS Nano*, 2013, **7**(8), 6875–6883.
44 W.-h. Li, Q.-y. Yue, Z.-h. Ma, B.-y. Gao, Y.-j. Li and H.-x. Zhao, *Water Sci. Technol.*, 2013, **67**(2), 284–292.